Bao *et al.*
Chinese Journal of Mechanical Engineering (2024) 37:12
https://doi.org/10.1186/s10033-024-00994-x

Chinese Journal of Mechanical Engineering

ORIGINAL ARTICLE

Open Access

A Modified Iterative Learning Control Approach for the Active Suppression of Rotor Vibration Induced by Coupled Unbalance and Misalignment

Yifan Bao[1,2], Jianfei Yao[1,2,3,4*], Fabrizio Scarpa[5,6] and Yan Li[2,3,4]

Abstract

This paper proposes a modified iterative learning control (MILC) periodical feedback-feedforward algorithm to reduce the vibration of a rotor caused by coupled unbalance and parallel misalignment. The control of the vibration of the rotor is provided by an active magnetic actuator (AMA). The iterative gain of the MILC algorithm here presented has a self-adjustment based on the magnitude of the vibration. Notch filters are adopted to extract the synchronous ($1\times\boldsymbol{\Omega}$) and twice rotational frequency ($2\times\boldsymbol{\Omega}$) components of the rotor vibration. Both the notch frequency of the filter and the size of feedforward storage used during the experiment have a real-time adaptation to the rotational speed. The method proposed in this work can provide effective suppression of the vibration of the rotor in case of sudden changes or fluctuations of the rotor speed. Simulations and experiments using the MILC algorithm proposed here are carried out and give evidence to the feasibility and robustness of the technique proposed.

Keywords Rotor vibration suppression, Modified iterative learning control, Unbalance, Parallel misalignment, Active magnetic actuator

1 Introduction

Rotating machinery often operates in harsh conditions and it is subjected to various periodic excitations. Rotor vibration caused by coupled faults is difficult to analyze and often leads to critical dynamic conditions with potential losses in terms of efficiency of the rotor system and/or global failure. A significant body of research has been dedicated to the investigation into active control of rotor vibrations. Examples of active control devices used for this purpose are active gas bearing [1], actuators based on magnetorheological fluids [2, 3], shear thickening fluids [4], shape memory alloy metal [5, 6] and piezoelectric actuators [7].

Active magnetic actuators (AMAs) have been widely applied to the active control of rotor vibration. AMAs are non-contact devices that also possess no wear, no sealing, absence of lubrication and low levels of losses [8, 9]. A significant body of research has been recently focused

*Correspondence:
Jianfei Yao
yaojf@mail.buct.edu.cn
[1] College of Mechanical and Electrical Engineering, Beijing University of Chemical Technology, Beijing 100029, China
[2] State Key Laboratory of High-end Compressor and System Technology, Beijing 100029, China
[3] Beijing Key Laboratory of High-end Mechanical Equipment Health Monitoring and Self-Recovery, Beijing University of Chemical Technology, Beijing 100029, China
[4] Key Lab of Engine Health Monitoring-Control and Networking of Ministry of Education, Beijing University of Chemical Technology, Beijing 100029, China
[5] Bristol Composites Institute (ACCIS), University of Bristol, Bristol BS8 1TR, UK
[6] Dynamics and Control Research Group (DCRG), University of Bristol, Bristol BS8 1TR, UK

on the use of electromagnetic bearings or actuators to suppress the vibration of rotors. The vibration caused by the rotor unbalance can be suppressed using AMAs. Fang et al. have designed a feedforward controller to suppress the vibration caused by rotor unbalanced with the active magnetic bearings (AMBs) [10]. Feng et al. have proposed a feedforward control strategy combined with a novel adaptive notch filter to solve problems caused by rotor unbalance in high-speed magnetic suspension centrifugal compressors [11]. Heindal et al. have found a closed-form analytical solution for the elimination of unbalance-induced bearing force on arbitrary, gyroscopic rotors [12]. Chen et al. have proposed an adaptive unbalance compensation scheme based on the theory of immersion and invariance control [13]. Shao et al. have designed an active fast imbalance vibration control method based on the principle of feedforward compensation and self-optimization [14]. For the rotor vibration due to misalignment, Inayat-Hussain has investigated the response of a statically misaligned flexible rotor mounted using AMBs and analyzed a rich variety of nonlinear phenomena and characteristics in the response [15]. Bouaziz et al. have presented three simplified models representing misaligned rotors mounted in current-biased radial AMBs and investigated the dynamic response of those systems [16]. Kumar et al. have proposed a novel trial misalignment approach and identification algorithm to solve the problem of misaligned rotors [17]. More studies about vibration control of rotors subjected to single excitation are available in open literature; a noticeable lower number of works about the case multiple excitations is however found. Jiang et al. have proposed a method based on an adaptive finite-duration impulse response filter in time domain for the suppression of vibration induced by multiple frequencies periodic excitations, and the technique makes use of AMBs [18]. Yao et al. have proposed a method to control the multiple frequencies periodic vibration of a rotor based on on-line self-optimizing algorithms [19].

One of the most evident characteristics of the vibration of the rotor is its periodicity, which is generally related to the frequency of rotation $\boldsymbol{\Omega}$. For example, the unbalanced vibration mode of the rotor is proportional to the shape of a $1\times\boldsymbol{\Omega}$ frequency sine wave, and the waveform of the parallel misalignment vibration is mainly dominated by the $2\times\boldsymbol{\Omega}$ frequency component [20]. When two different types of vibration exist at the same time, the resulting dynamic displacement of the rotor is a coupling of the $1\times\boldsymbol{\Omega}$ and $2\times\boldsymbol{\Omega}$ waveforms. In 1978, Uchiyama proposed the concept of learning control based on the periodic characteristics of a high-speed manipulator. Arimoto et al. have developed Uchiyama's ideas and formally put forward the concept of iterative learning control (ILC), which has received widespread attention within the community [21]. Costic et al. have operated active magnetic bearings using the ILC strategy to conduct studies about the compensation of a rotor unbalance [22]. Chiacchiarin and Mandolesi have introduced the concept of forgetting factor and noncausal low-pass filter in the ILC algorithm. Those Authors also provided experimental evidence of the significant control effect that the modified ILC algorithm could provide in compensating the vibration generated by rotor unbalance [23]. Bi et al. have then proposed an automatic learning control algorithm that employs variable learning cycles and gains to optimize control currents for the compensations of the unbalance; the algorithm is effective over a wide range of operational speeds [24]. Gao et al. have introduced an impact factor to enhance the convergence speed and proposed an adaptive iterative learning control scheme [25]. Recently, Tang et al. have used an extended state observer to estimate and attenuate the disturbances in every iteration of ILC [26]. Zheng et al. have proposed an ILC algorithm based on the system information of the iteration before the last to solve the packet loss problem encountered in real-time control [27]. Those Authors have also simplified the Newton-type ILC algorithm and combined it with a model-free control method [28]. Sun et al. have proposed a modified iterative learning control strategy for magnetic bearing systems to reject the disturbance based on an extended state observer [29].

In this work, we employ an active magnetic actuator as a control device to reduce the periodic vibration of the rotor caused by the coupling between rotor unbalance and rotor misalignment. A finite element model of the rotor-bearing-AMA system including unbalance and parallel misalignment features is first established. A ILC scheme is adopted as the control law is then adopted. The ILC focuses on the periodic characteristics of the vibration of the rotor and an adaptive factor $\boldsymbol{\sigma}$ is introduced to modify the arithmetic of the algorithm. The ILC scheme is subsequently modified again to counteract the adverse effect of experimental features affecting the control and stability of the algorithm. Finally, simulations and experiments are performed to verify the feasibility of our modified iterative learning control (MILC).

2 Method

2.1 Dynamics Modeling

The system of equations of motions related to rotor-bearing system with AMA is formulated as follows:

$$\boldsymbol{M}\ddot{\boldsymbol{Z}} + \boldsymbol{C}\dot{\boldsymbol{Z}} + \boldsymbol{K}\boldsymbol{Z} = \boldsymbol{F}, \tag{1}$$

$$\boldsymbol{F} = \boldsymbol{F}_1 + \boldsymbol{F}_2, \tag{2}$$

where $\boldsymbol{M}$, $\boldsymbol{C}$, $\boldsymbol{K}$ are the mass, damping and stiffness matrices of the rotor system. The generalized displacement vector is $\boldsymbol{Z}$, $\boldsymbol{F}$ is the generalized force that includes the active control force $\boldsymbol{F}_2$, which is the electromagnetic force of the AMA, and the interference force $\boldsymbol{F}_1$. The latter is composed by the unbalanced force $\boldsymbol{F}_\mathrm{d}$, and the parallel misaligned force, $\boldsymbol{F}_\mathrm{c}$.

The unbalanced force at the node of the disk can be expressed as:

$$\boldsymbol{F}_\mathrm{d} = m_\mathrm{d}\omega^2 e\left[\begin{array}{cc}\cos(\omega t+\gamma) & \sin(\omega t+\gamma)\end{array}\right]^\mathrm{T}, \tag{3}$$

where m_d is the mass of the disk, ω is the rotate speed, e is the mass eccentricity at the disk and γ is the phase angle of the mass eccentricity.

A parallel misalignment force is also considered in rotor shaft systems. The rigid coupling in the rotor-shaft system is formulated using the method of the equivalent shaft segments [20]. The resulting expression of the misalignment force is:

$$\boldsymbol{F}_\mathrm{c} = \frac{k_\mathrm{c}\delta}{4}\left[\begin{array}{c}\sin(2\omega t)\\ 1+\cos(2\omega t)\end{array}\right], \tag{4}$$

where δ is the deviation of the centering and k_c is the radial stiffness of the coupling.

The unbalanced and the parallel misalignment forces can be integrated into the global coordinates of the system through the transformation matrices $\boldsymbol{T}_\mathrm{d}$ and $\boldsymbol{T}_\mathrm{c}$ of the corresponding nodes. The generalized interference force in Eq. (2) is therefore obtained as:

$$\boldsymbol{F}_1 = \boldsymbol{T}_\mathrm{d}^\mathrm{T}\boldsymbol{F}_\mathrm{d} + \boldsymbol{T}_\mathrm{c}^\mathrm{T}\boldsymbol{F}_\mathrm{c}. \tag{5}$$

The single degree-of-freedom electromagnetic force (for example along the X direction) is:

$$F_\mathrm{mag}^x = k\frac{i_x^2}{s^2}, \quad k = \frac{\mu_0 N_0 A}{4}, \tag{6}$$

where μ_0 is the magnetic permeability in vacuum, N_0 is the number of the coil turns, A is the magnetic pole area and s is the air gap.

The equation representing the electromagnetic force is a binary non-linear function relating displacement and current. The electromagnetic force is expanded and linearized around the operational point by Taylor expansion. The electromagnetic force can be therefore simplified as:

$$F_\mathrm{mag}^x = -k_s\boldsymbol{x} + k_i i_x, \tag{7}$$

where i_0 is the bias current, k_s is the displacement stiffness ($k_s = \mu_0 N_0^2 A i_0^2/s^3$) and k_i is the current stiffness ($k_i = \mu_0 N_0^2 A i_0/s^2$).

Assuming that the air gaps along the horizontal and vertical directions are uniform and the areas of all magnetic poles are the same, and regardless of the magnetic field coupling and the magnetic flux leakage effects in both directions, the displacement and current stiffness along the horizontal and vertical directions can be assumed as being equal. The control force $\boldsymbol{F}_\mathrm{a}$ can be partitioned in the following way related to the working node:

$$\begin{aligned}\boldsymbol{F}_\mathrm{a} &= \left[\begin{array}{cc}F_\mathrm{mag}^x & F_\mathrm{mag}^y\end{array}\right]^\mathrm{T} = -k_s\left[\begin{array}{c}\boldsymbol{x}\\ \boldsymbol{y}\end{array}\right] + k_i\left[\begin{array}{c}i_x\\ i_y\end{array}\right]\\ &= -k_s\boldsymbol{z}_\mathrm{a} + k_i\boldsymbol{i}_\mathrm{a}.\end{aligned} \tag{8}$$

The disturbance force or the control force in the local coordinate system needs to be converted into the global coordinate system by the transformation matrix. Taking the electromagnetic force as an example, by using the transformation matrix $\boldsymbol{T}_\mathrm{a}$ one obtains:

$$\boldsymbol{F}_2 = \boldsymbol{T}_\mathrm{a}^\mathrm{T}\left\{k_s\boldsymbol{T}_\mathrm{a}\boldsymbol{z}_\mathrm{a} + k_i\boldsymbol{i}_\mathrm{a}\right\}. \tag{9}$$

Transformation of Eq. (1) leads to:

$$\begin{aligned}&\boldsymbol{M}\ddot{\boldsymbol{Z}} + \boldsymbol{C}\dot{\boldsymbol{Z}} + \left\{\boldsymbol{K} + k_s\boldsymbol{T}_\mathrm{a}^\mathrm{T}\boldsymbol{T}_\mathrm{a}\right\}\boldsymbol{Z}\\ &= \boldsymbol{F}_1 + k_i\boldsymbol{T}_\mathrm{a}^\mathrm{T}\boldsymbol{i}_\mathrm{a}.\end{aligned} \tag{10}$$

The new stiffness matrix is set as $\boldsymbol{K}_1$:

$$\boldsymbol{K}_1 = \boldsymbol{K} + k_s\boldsymbol{T}_\mathrm{a}^\mathrm{T}\boldsymbol{T}_\mathrm{a}. \tag{11}$$

The equations of motions are transformed into finite element discretization that needs to be transformed into a state space equation for solving the transient motion. The state space vector is defined as:

$$\boldsymbol{q} = \left[\begin{array}{c}\boldsymbol{Z}\\ \dot{\boldsymbol{Z}}\end{array}\right], \quad \dot{\boldsymbol{q}} = \left[\begin{array}{c}\dot{\boldsymbol{Z}}\\ \ddot{\boldsymbol{Z}}\end{array}\right]. \tag{12}$$

The matrix $\ddot{\boldsymbol{Z}}$ is obtained via Eq. (12):

$$\begin{aligned}\ddot{\boldsymbol{Z}} &= \boldsymbol{M}^{-1}\boldsymbol{F}_1 + \boldsymbol{M}^{-1}\left\{k_i\boldsymbol{T}_\mathrm{a}^\mathrm{T}\boldsymbol{i}_\mathrm{a}\right\}\\ &\quad - \boldsymbol{M}^{-1}\boldsymbol{C}\dot{\boldsymbol{Z}} - \boldsymbol{M}^{-1}\boldsymbol{K}_1\boldsymbol{Z}.\end{aligned} \tag{13}$$

By transforming the Eq. (13) into the form of the first order differential equation one obtains:

$$\begin{aligned}\left[\begin{array}{c}\dot{\boldsymbol{Z}}\\ \ddot{\boldsymbol{Z}}\end{array}\right] &= \left[\begin{array}{cc}0 & \mathrm{I}\\ -\boldsymbol{M}^{-1}\boldsymbol{K}_1 & -\boldsymbol{M}^{-1}\boldsymbol{C}\end{array}\right]\left[\begin{array}{c}\boldsymbol{Z}\\ \dot{\boldsymbol{Z}}\end{array}\right]\\ &\quad + \left[\begin{array}{cc}0 & \boldsymbol{M}^{-1}\end{array}\right]^\mathrm{T}k_i\boldsymbol{T}_\mathrm{a}^\mathrm{T}\boldsymbol{i}_\mathrm{a} + \left[\begin{array}{cc}0 & \boldsymbol{M}^{-1}\end{array}\right]^\mathrm{T}\boldsymbol{F}_1.\end{aligned} \tag{14}$$

Substituting Eq. (12) into the Eq. (14) the state space formulation can be abbreviated as [30]:

$$\dot{\boldsymbol{q}} = \boldsymbol{A}_\mathrm{s}\boldsymbol{q} + \boldsymbol{B}_\mathrm{sa}\boldsymbol{i}_\mathrm{a} + \boldsymbol{B}_\mathrm{su}\boldsymbol{F}_1, \tag{15}$$

where $\boldsymbol{A}_{\mathrm{s}}$ is the system matrix, $\boldsymbol{B}_{\mathrm{sa}}$ is the input matrices of the AMA current and $\boldsymbol{B}_{\mathrm{su}}$ are the input matrices of the interference force.

2.2 Control Law Design

The ILC algorithm is a typical periodic feedforward control scheme and it is significantly valid for periodic vibrations of the rotor. As example, the P-type ILC strategy is formulated as [31]:

$$\begin{cases} v_{k+1}(n) = v_k(n) + Pe_k(n), \\ e_k(n) = y_d(n) - y_k(n), \end{cases} \quad n \in [0, N], \tag{16}$$

where k is the number of iteration periods, n is the correspondent point in time for each iterative period, $e_k(n)$ is the vibration error, P is the proportional learning gain and N is the memory size.

The basic principle of the algorithm is to superimpose $Pe_k(n)$ on the output control $v_k(n)$ at the time n of the cycle and to take this value as the output control $v_{k+1}(n)$ at the same time n of the next cycle. Two key aspects need to be considered for the implementation of the ILC scheme:

(1) The design of the superimposed control quantity of the algorithm, such as the proportion-type law ($Pe_k(n)$) and the differential-type law ($D\dot{e}_k(n)$);
(2) During the actual application of the control scheme, not only the impact of the noise needs to be considered, but also the fluctuation of the rotational speed frequency f and the sampling frequency f_s must also be considered. The frequency f and f_s will affect the size of the memory $N = \mathrm{int}(f_s/f)$ and therefore the performance of the controller. Moreover, a fixed-size memory N does not meet the requirements for an effective multi-speed control.

Based on the two critical points raised above, we propose a novel modified iterative learning control scheme for the active vibration suppression of a rotor with coupled unbalance and misalignment.

2.2.1 Modified Point I for ILC Algorithm

The selection of the parameters for the ILC algorithm has always been one of the main difficulties to operate the PID-type ILC strategy. Although by increasing the proportional learning gain P one could improve the speed of convergence, large values of P will also lead to unstable control. One of the critical aspects of the ILC methodology is indeed how to keep a balance between the convergence speed and convergence performance. The design of adaptive ILC schemes is mostly focused on establishing variable forgetting factor functions [25] or variable gain functions [27, 28] with the iteration cycle k, or to build look-up tables [24]. In this work, an adaptive factor σ based on the error value $|e_k(n)|$ is introduced to enhance the robustness and the stability of the ILC method, with a resulting gain scheduling control. As an adjustment factor used in the iterative learning process, the factor σ increases as the error value increases. At the same time, σ decreases when the value of the error becomes smaller. Eqs. (17) and (18) show the specific control law used for this MILC algorithm:

$$v_{k+1}(n) = v_k(n) + P\sigma e_k(n), \quad n \in [0, N], \tag{17}$$

$$\sigma = 1 - \alpha \exp(-\beta |e_k(n)|), \tag{18}$$

where the adjustable parameters $\alpha = 0$ or 1, $\beta \in [0,1]$. When $\alpha = 0$, Eq. (17) becomes a classical ILC formulation.

The effective calculation of Eq. (18) involves considerable CPU time during the actual operation. It is also significantly easier to use integer arithmetic in the field programmable gate array (FPGA). Eq. (18) can be therefore improved as follows:

$$\sigma = 1 - \alpha 2^{-\mathrm{round}(\beta |\bar{e}_k(n)|)}, \tag{19}$$

where round $(\cdot)$ is the rounding function and $\bar{e}_k(n) = e_k(n) \times 10^6$. The variation of the adaptive gain $P\sigma$ with $|e_k(n)|$ is shown in Figure 1 when $|e_k(n)|$ changes from 0 to 25 μm. Based on the magnitude of the vibration, which is not hard to obtain, the adaptive law can be expediently designed by adjusting parameters P, α and β.

2.2.2 Modified Point II for ILC Algorithm

Some inevitable phenomena associated to noise, irregular rotating speed and unstable sampling rate are encountered within normal operations for rotating machinery systems. These factors impact in a very

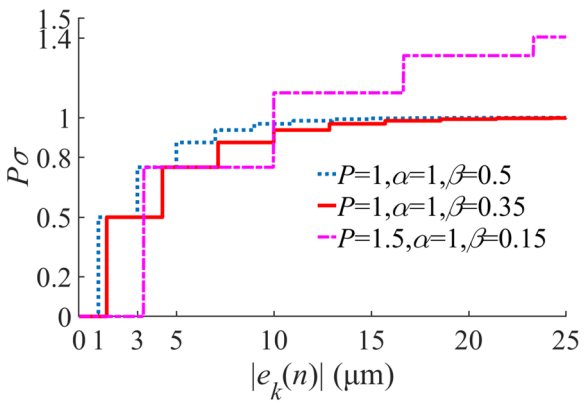

Figure 1 Adaptive factor σ

significant way the stability and robustness of periodic feedforward algorithms, such as the ILC one. On the basis of the algorithm described in Section 2.2.1, we propose two further measures to improve the proposed algorithm for realistic operations:

(1) We take into account the influence of the fluctuations of the rotating speed frequency f and sampling frequency f_s on the memory size N by using a feedback loop to update the memory size N in real time and adjusted according to the variations of f and f_s.
(2) Notch filters are adopted to extract the $1\times\boldsymbol{\Omega}$ and $2\times\boldsymbol{\Omega}$ frequency components to eliminate the influence of noise. In addition, the notch frequency f_n and $2f_n$ could also be adjusted real-time change with the rotating speed frequency f by the feedback loop mentioned in (1) to meet the requirements of multi-speed control.

The MILC formulation expressed in Eq. (17) is in essence a feedforward control strategy.In this paper, a parallel proportional feedback loop is added to the MILC formulations. The block diagram of the MILC system is shown in Figure 2. The $1\times\boldsymbol{\Omega}$ and $2\times\boldsymbol{\Omega}$ frequency components of the system error $e_k(n)$ are extracted through the notch filter, and the total output control $u_k(n)$ is obtained by the MILC feedforward loop and the parallel feedback loop. The expression of $u_k(n)$ is:

$$\begin{aligned} u_k(n) &= v_k^f(n) + P_1 e_k(n)_{f_n} + P_2 e_k(n)_{2f_n} \\ &= v_k^f(n) + u_k^b(n)_{f_n} + u_k^b(n)_{2f_n}. \end{aligned} \tag{20}$$

The feedback controller in Eq. (20) is divided into proportional controllers I and II according to the frequency component. The quantity $v_k^f(n)$ is the output of the feedforward control, $u_k^b(n)$ is the output of feedback control and P_1 and P_2 are the feedback gain of $1\times\boldsymbol{\Omega}$ and $2\times\boldsymbol{\Omega}$ frequency components. If $P_1=P_2$, the proportional controllers I and II shown in Figure 2 could be treated as one controller.

2.3 Convergence Analysis

To understand better the functioning of the MILC algorithm, the control output is written as:

$$\begin{aligned} u_k(n) &= c_k(n) + v_k(n) = K_\mathrm{p} e_k(n) \\ &\quad + P[1 - \alpha \exp(-\beta e_{k-1}(n))] e_{k-1}(n) \end{aligned} \tag{21}$$

where $u_k(n)$ is the control output, $c_k(n)$ is the proportional controller output, K_p is the proportional gain and $v_k(n)$ is the feedforward controller output.

The error signal function can be obtained from Eq. (21) as:

$$e_k(n) = \frac{u_k(n) - v_k(n)}{K_\mathrm{p}}. \tag{22}$$

Putting Eq. (22) into Eq. (17), one obtains:

$$\begin{aligned} v_{k+1}(n) = v_k(n) - \frac{P}{K_\mathrm{p}} \left\{ 1 - \alpha \exp\left(\frac{\beta}{K_\mathrm{p}} [v_k(n) - u_k(n)]\right) \right\} \\ \times [v_k(n) - u_k(n)]. \end{aligned} \tag{23}$$

The transformation of the limit about the iterative number k at two sides of Eq. (23) is given by:

$$\begin{aligned} \lim_{k\to\infty} v_{k+1}(n) = v_\infty(n) = \lim_{k\to\infty} v_k(n) - \frac{P}{K_\mathrm{p}} \lim_{k\to\infty} [v_k(n) - u_k(n)] \\ \times \left\{ 1 - \alpha \exp\left(\frac{\beta}{K_\mathrm{p}} \lim_{k\to\infty} [v_k(n) - u_k(n)]\right) \right\}. \end{aligned} \tag{24}$$

If α=0 or 1, Eq. (24) can be further simplified as:

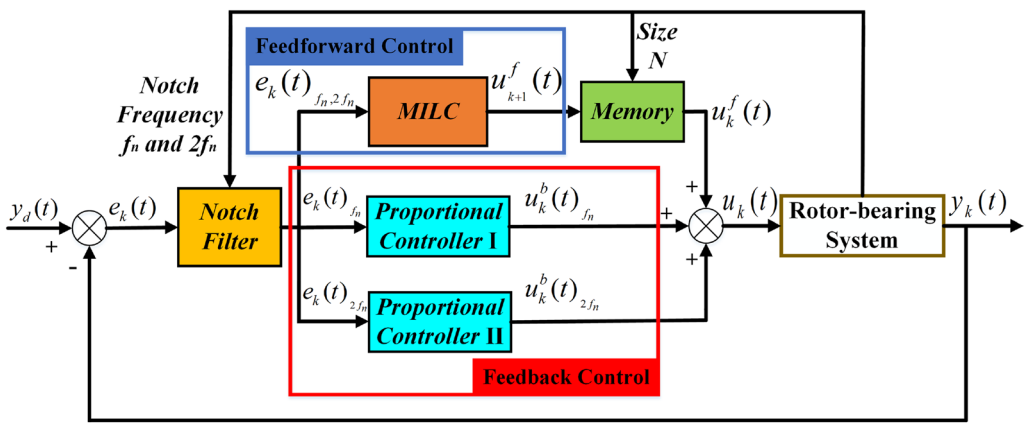

Figure 2 Block diagram of the MILC system

$$\lim_{k\to\infty}[v_k(n)-u_k(n)]=0. \tag{25}$$

According to Eqs. (22) and (25), the error signal $e_k(n)$ can therefore be written as:

$$\lim_{k\to\infty} e_k(n)=\frac{\lim\limits_{k\to\infty}[u_k(n)-v_k(n)]}{K_p}=0. \tag{26}$$

Thus, the convergence of MILC can be demonstrated by Eqs. (25) and (26).

3 Numerical and Experimental Work

3.1 Description and Modeling of Test Rig

The test rig of the rotor-bearing-AMA system is shown in Figure 3. The test rig is mainly composed of a rotating shaft, disk, coupling, tilting-pad journal bearings (TPJBs), AMA, sensors, data acquisition system, control system and motor drive system. The temperature and operating pressure of ISO VG32 lubricating oil are 20 °C and 0.2 MPa, respectively. Four measuring points are present and they are provided with six eddy current displacement proximity probes. The probe of measuring point #1 is to measure the real-time speed; the other probes are used to measure the displacement of the rotor. The sampling frequency of the data acquisition system is 10.24 kHz. The specific parameters of the test rig are shown in Table 1.

A finite element method is used to simulate the rotor and the actuator system (Figure 4). The numerical model of the rotor is divided into 11 elements which adopt Timoshenko beam structure. The model includes coupling, shaft, bearings, AMA and the disc. The parameters of model are consistent with the test rig shown in Table 1. The material damping of the shaft is not considered. The unbalanced force is exerted at node #9 where the disc is located, and the misaligned force is on node #3. The actuator adopts a 12-pole E-type structure and generates active control force acting on node #7.

Table 1 Parameters of the test rig

Type	Item	Value
AMA	Number of turns N_0	175
	Magnetic pole area A (m^2)	10^{-4}
	Rotor-stator clearance s (mm)	0.6
	Rotor diameter (mm)	125
	Stator diameter (mm)	126.2
Rotor	Length of shaft (m)	1
	Outer diameter (mm)	50
	Thickness of disc (mm)	25
	Diameter of disc (mm)	270
TPJBs	Number of pads	5
	Clearance (mm)	0.05
	Preload	0.2
Coupling	Half coupling length (mm)	65

3.2 Simulation Results

Simulations are first carried out to verify the effectiveness of the MILC strategy on controlling the rotor vibration due to the presence of coupled unbalance and misalignment. The simulations are only performed here to assess the validity of the proposed algorithm, and the parameters used are slightly different from those of the experiment. The sampling frequency f_s is 10 kHz, the rotating speed frequency f is 100 Hz, the feedforward gain of the MILC parameter P is 6×10^6, the feedback gains P_1 and P_2 both are 10^6 and the adjustable parameters are $\alpha=1$, $\beta=0.5$. The control is applied after 0.2 s of the rotor running.

The simulation results from node #7 before and after controller activation are shown in Figure 5. Figure 5(a) and (b) represent the orbit of the rotor center and the frequency domain response, respectively. It can be seen from Figure 5(a) and (b) that the orbit of the rotor is closer to the origin of the coordinates after control, and the $1\times\boldsymbol{\Omega}$ and $2\times\boldsymbol{\Omega}$ frequency components both are suppressed. This confirms that the controller can significantly reduce the amplitude of the vibration. Figure 5(c) is the diagram of the self-adjust gain $P\sigma$

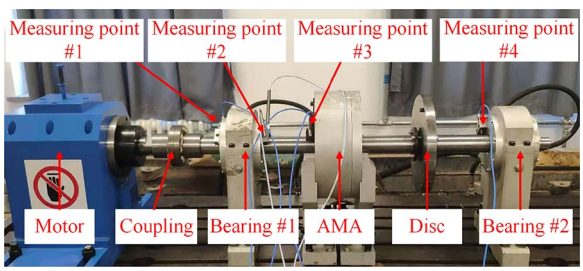

Figure 3 Test rig of rotor-bearing-AMA system

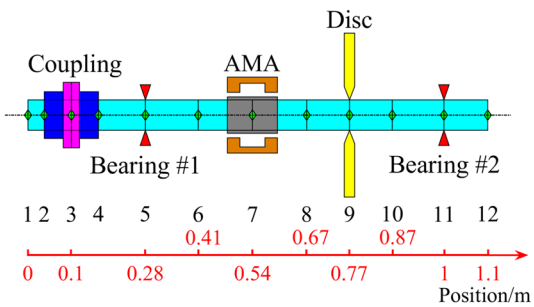

Figure 4 Model of rotor-bearing-AMA system

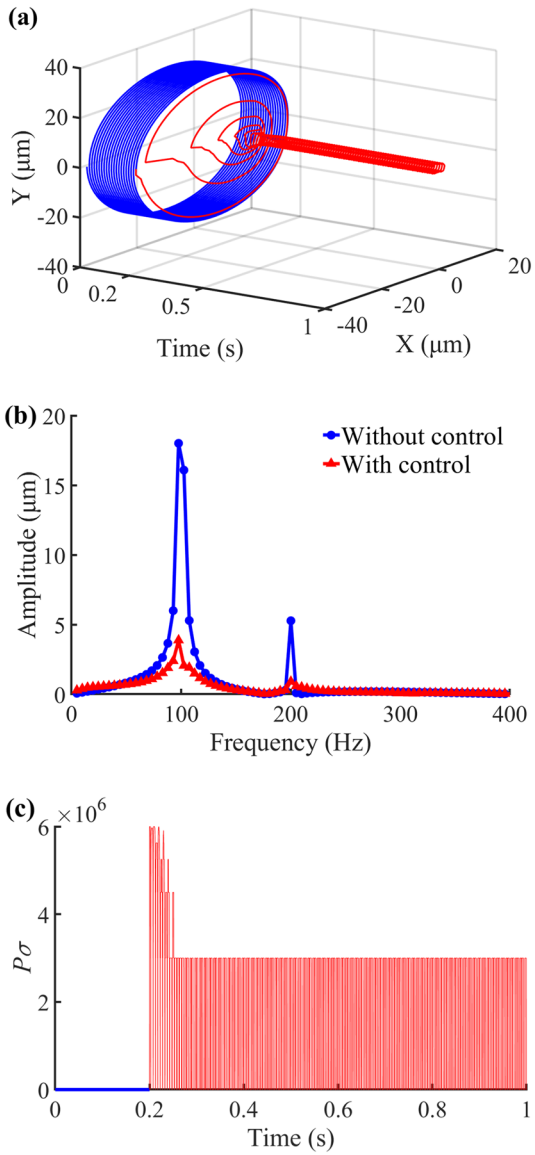

Figure 5 Simulation results from node #7: (**a**) Orbit of the rotor center, (**b**) Frequency domain response, (**c**) Diagram of the self-adjust gain *Pσ*

and the self-adjust factor σ affects the function of the threshold switch control via the adjustable parameters α and β. When $|e_k(n)|$ is small, $P\sigma=0$.

3.3 Experimental Tests

The evaluation of the real-time rotor vibration mitigation was carried out at speeds of 900 r/min, 1050 r/min, 1200 r/min, 1350 r/min, 1500 r/min, 1650 r/min, 1800 r/min and 1990 r/min. A comparison between the stability performance provided by the MILC algorithm and a traditional ILC approach was also performed. Experiments using the proposed control method have been also carried out under spin speed changes and fluctuations. In these cases, during the control process the rotor speed has been increased (1650 r/min→1800 r/min) and decreased (1500 r/min→1350 r/min).

3.3.1 Experimental Results at Different Rotor Speed

Figures 6 and 7 show the experimental result related to rotational speed of 1350 r/min and 1800 r/min. The control force is applied after 20 s of the rotor running. The time domain waveform diagrams (a), (b) and (c) of the measurement points #2, #3 and #4 are plotted using notch filters to extract the $1\times\boldsymbol{\Omega}$ and $2\times\boldsymbol{\Omega}$ frequency components from the measurement points. The amplitude of each measurement point at 1350 r/min is reduced by approximately 63% (#2), 72% (#3) and 49% (#4), while different rates of reduction are observed at 1800 r/min (68% for #2, 72% for #3 and 45% for #4). These results prove the general validity of the proposed control algorithm. Figure 6(d) and 7(d) shows the spectral waterfall of the AMA's measurements with and without control: noise is present at each frequency. Although the noise is not large compared to the amplitude of the system at the fault frequency, the accumulated noise still significantly affects the control performance, which is also one of the reasons behind the adoption of notch filters in this work. The rotor system works in harsh operating conditions in practical applications, and noise of its vibration signal is also evident. It can be found that both the $1\times\boldsymbol{\Omega}$ and $2\times\boldsymbol{\Omega}$ frequency components of the rotor vibration are suppressed after control, which confirms the effectiveness of the MILC algorithm when unbalance and parallel misalignment occur. Figure 6(e) and 7(e) show the waterfall of the $1\times\boldsymbol{\Omega}$ and $2\times\boldsymbol{\Omega}$ frequency components with notch filters extracted in real-time. The effect of the filters is quite evident.

The rotor vibration is strongly limited at different rotor speeds. Figure 8 shows the amplitude of measurement point #3 before and after control. The experimental results demonstrate that the proposed strategy is valid for the rotor-bearing-AMA system at different speed conditions and the reduction of the amplitude of point #3 is between 71.3% and 79.6% at the various speeds considered.

3.3.2 Experimental Comparison between MILC with ILC

The adaptive factor σ shown in Figure 1 provides a better reference to select the adjustable parameters α and β when the amplitude of the vibration is about (or larger than) 25 μm. The experimental parameters shown in Table 2 are adopted to compare and assess the influence of the large initial gain P on the stability of the control algorithm. Figures 9 and 10 represent the vibration

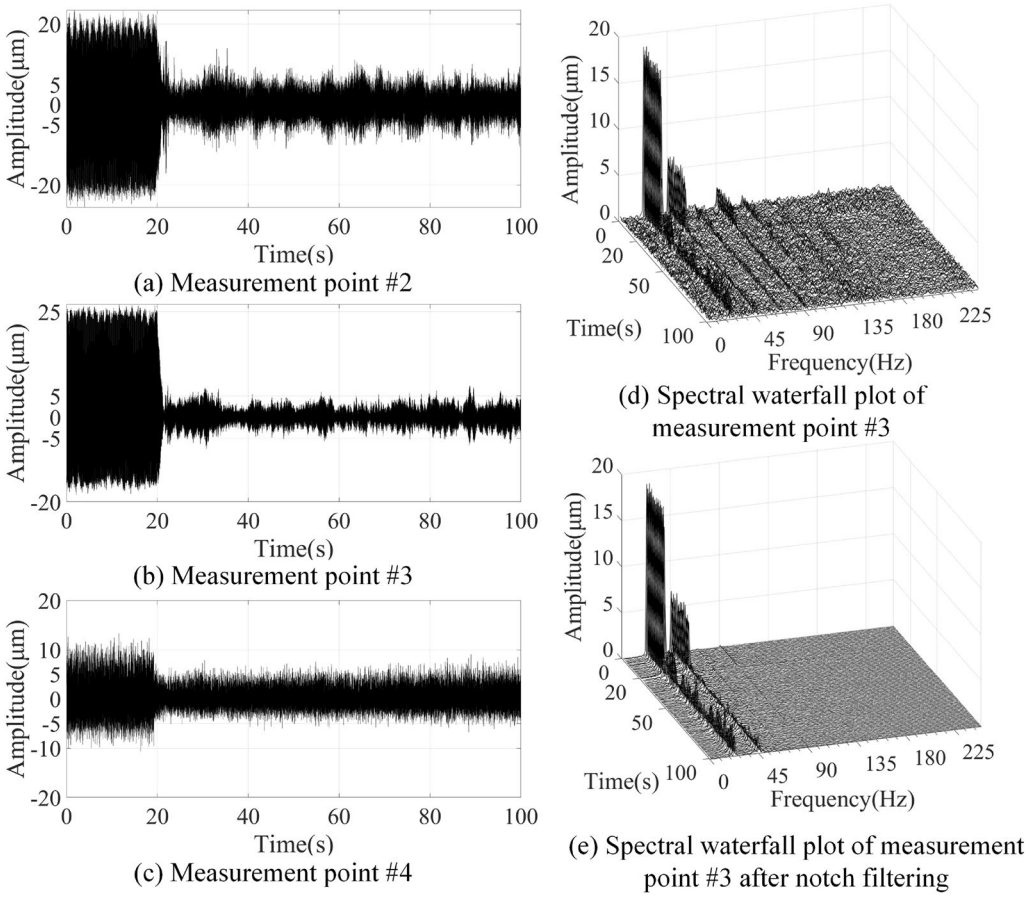

Figure 6 Experimental results at speed of 1350 r/min

waveform of the two sets of experiments at measurement #3 before and after controller activation. It is worth noting again that when α=0, the MILC algorithm is equivalent to the typical ILC arithmetic. The other parameters of two experimental groups are the same, with bias current $i_0=1$ A, $P_x=2000$, $f=f_n=27.5$ Hz, $P_{1x}=P_{1y}=10^4$, $P_{2x}=0$ and $P_{2y}=2\times10^4$.

Figure 9 shows the experimental results of Group 1. The value of the initial gain P is 5000 and the control force is applied at 10 s. The ILC and MILC algorithms both quickly converge. The ILC-controlled rotor however starts to diverge ~ 10 s after control is applied. The MILC strategy can still achieve a satisfactory stability control due to the adaptive factor σ. The value of $P\sigma$ has a similar trend with the curve in Figure 5(c); a $P\sigma=0$ means that the amplitude is under threshold, $u_{k+1}(n)=u_k(n)$.

Figure 10 shows the results associated to Group 2. The control provided through ILC strategy is not ideal when the value of the initial gain P is 6000 and the amplitude fluctuates within ± 8 μm. Similarly, vibration controlled via MILC still provides initial fluctuations. The MILC algorithm however enables the gain to self-adjust during the $|e_k(n)|$ is preliminary suppressed and then provides a steady and significant control effect. The reduction of the feedforward gains is not permanent, which is very different from the design of the gain scheduling based on the iteration cycle k. The

Table 2 Parameters of experiments

Groups	P_y	α	β	Results
Group 1	5000	1	0.35	Figure 9
	5000	0	–	
Group 2	6000	1	0.5	Figure 10
	6000	0	–	

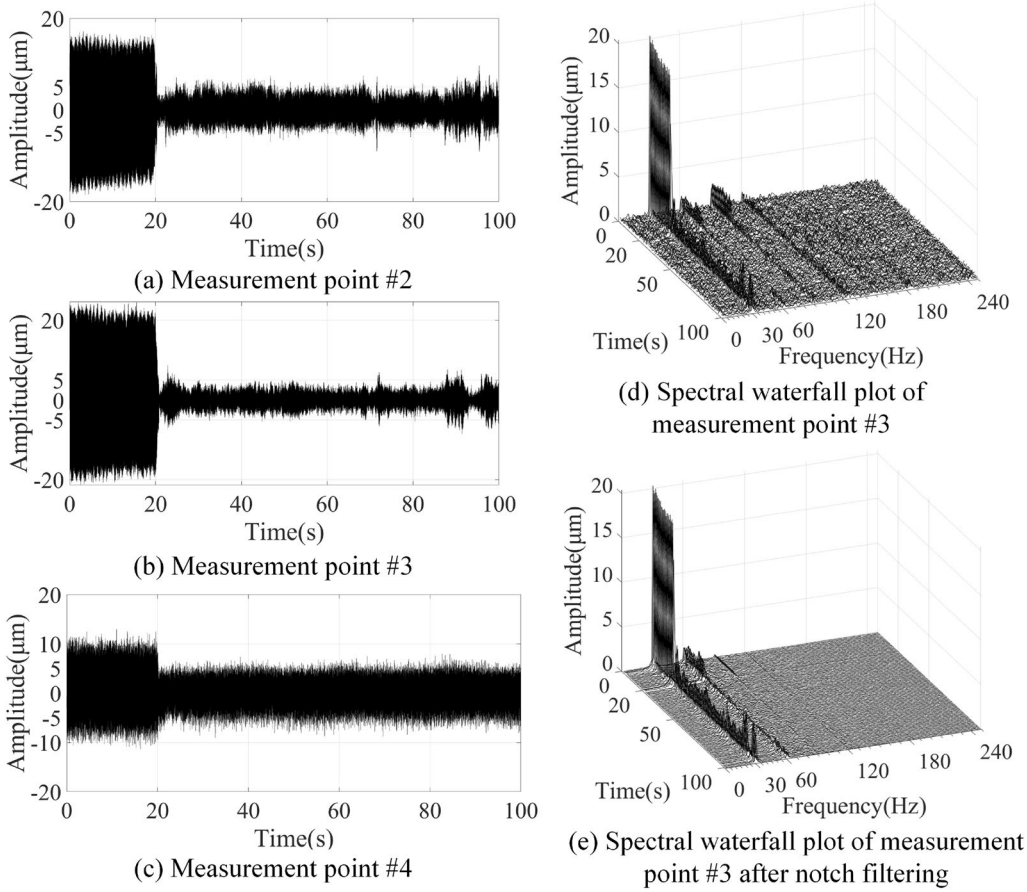

Figure 7 Experimental results at speed of 1800 r/min

system retains a periodical feedforward ability against sudden changes and fluctuations of the amplitude and is more suitable for complicated operational conditions in practical applications.

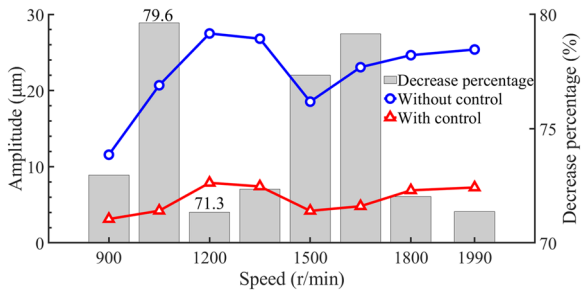

Figure 8 Comparison of different speed suppression effects at measure point #3

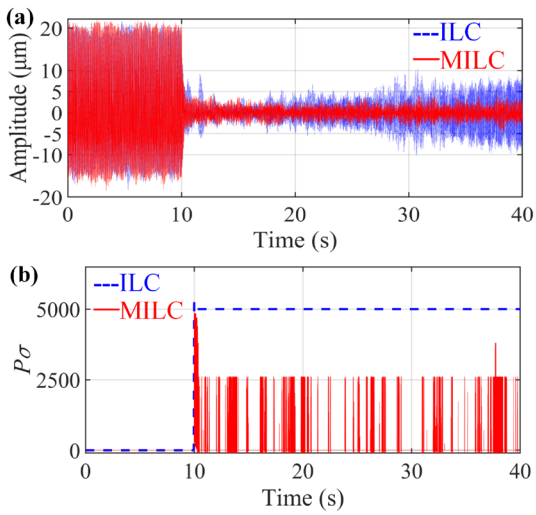

Figure 9 Experimental results of Group 1: (**a**) Vibration waveforms, (**b**) The self-adjust gain *Pσ*

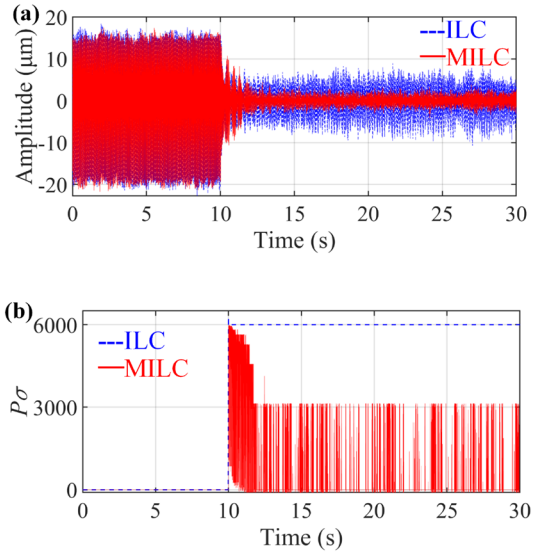

Figure 10 Experimental results of Group 2: (**a**) Vibration waveforms, (**b**) The self-adjust gain $P\sigma$

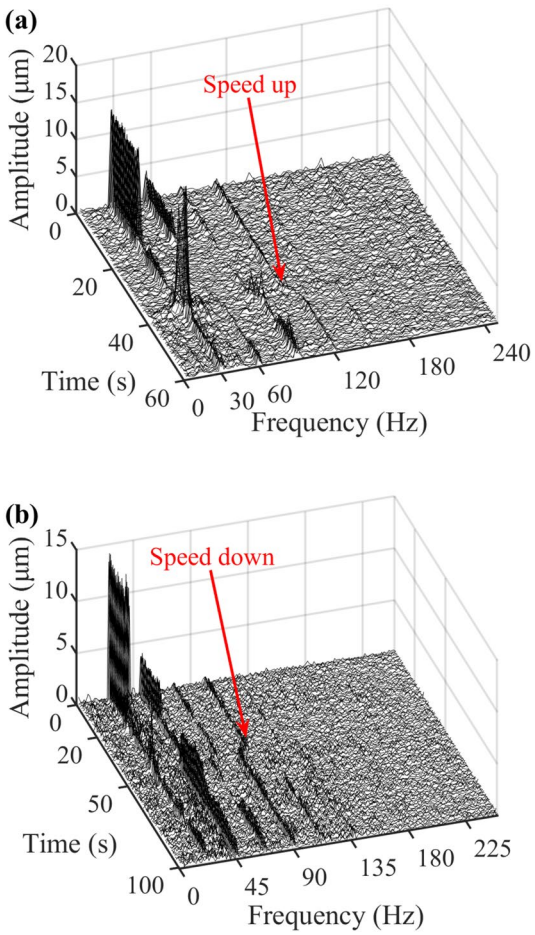

Figure 11 Experimental results related to speed changes: (**a**) The experimental group of speed up, (**b**) The experimental group of speed down

3.3.3 Rotor Speed Change and Fluctuation

In this case the rotating speed is increased from 1650 r/min to 1800 r/min during the control process. The resulting vibration of point #3 in the frequency domain is shown in Figure 11(a). Similarly, Figure 11(b) shows the results when the speed is reduced from 1500 r/min to 1350 r/min and the rotor speed changes are indicated by the red arrows. The self-adaptive notch filters and the periodic memory adjust the notch frequency f_n and the size of the memory N after the rotor speed changes. The experimental results shown in Figure 11 show that the MILC algorithm and its verification procedure could be applied efficiently in actual and realistic operational conditions.

4 Conclusions

This paper has presented a modified iterative learning control algorithm that could adjust the gain in an adaptive manner in light of the vibration errors $|e_k(n)|$. The proposed method is also further improved to consider the fluctuations of the rotating speed and the sampling frequency present in practical applications. Furthermore, notch filters are adopted to extract the $1\times\boldsymbol{\Omega}$ and $2\times\boldsymbol{\Omega}$ frequency components of the vibration to eliminate the influence of noise. Finally, a feedforward-feedback parallel control strategy is designed via combining the feedforward MILC algorithm with proportional feedback control. The following conclusions can be drawn:

(1) The proposed strategy has a significant impact on the reduction of the rotor vibration caused by coupling between unbalance and misalignment in multi-speed rotor systems. This method can be also extended to suppress multi-frequency vibration; this will however increase the computational effort during the real-time control;
(2) The MILC algorithm is more robust and stable than the ILC one because of the introduction of the adaptive factor σ and the improvements of the experimental procedure;
(3) The self-adaptability of notch filters and periodic memory ensures the stability of the controller against harsh operating conditions, especially when the rotating speed fluctuates. Nevertheless, because of the limitations of feedforward schemes, it is challenging to implement an effective inhibition if the speed variations are too rapid or too large in magnitude.

Acknowledgements
Not applicable.

Authors' Contributions
JY was in charge of the whole trial; YB and JY wrote the manuscript; FS assisted with Writing-Reviewing and Editing. YB and YL assisted with laboratory analyses and validation. All authors read and approved the final manuscript.

Funding
Supported by National Natural Science Foundation of China (Grant Nos. 51975037, 52375075).

Data availability
The data that support the findings of this study are available from the corresponding author, upon reasonable request.

Declarations

Competing Interests
The authors declare no competing financial interests.

Received: 15 March 2021 Revised: 28 December 2023 Accepted: 12 January 2024
Published online: 23 February 2024

References

[1] F G Pierart, I F Santos. Lateral vibration control of a flexible overcritical rotor via an active gas bearing – Theoretical and experimental comparisons. *Journal of Sound and Vibration*, 2016, 383: 20–34.
[2] J Zapoměl, P Ferfecki, J Kozánek. Modelling of magnetorheological squeeze film dampers for vibration suppression of rigid rotors. *International Journal of Mechanical Sciences*, 2017, 127: 191–197.
[3] L Ma, J Wang, C H Li. Vibration suppression of a rotor system with a nonlinear MR damper. *Archive of Applied Mechanics*, 2021, 91: 4053–4068.
[4] Q Zhao, J Yuan, H M Jiang, et al. Vibration control of a rotor system by shear thickening fluid dampers. *Journal of Sound and Vibration*, 2021, 494.
[5] Y H Ma, Q C Zhang, D Y Zhang, et al. Tuning the vibration of a rotor with shape memory alloy metal rubber supports. *Journal of Sound and Vibration*, 2015, 351: 1–16.
[6] S Enemark, I F Santos. Rotor-bearing system integrated with shape memory alloy springs for ensuring adaptable dynamics and damping enhancement—Theory and experiment. *Journal of Sound and Vibration*, 2016, 369: 29–49.
[7] M Shafiq, A Saleem, M Mesbah. Model-free data driven control for trajectory tracking of an amplified piezoelectric actuator. *Sensors and Actuators A: Physical*, 2018, 279: 27–35.
[8] G Schweitzer, E H Maslen. *Magnetic bearings theory, design, and application to rotating machinery*. Springer-Verlag Berlin Heidelberg, 2009.
[9] R S Srinivas, R Tiwari, C Kannababu. Application of active magnetic bearings in flexible rotordynamic systems – A state-of-the-art review. *Mechanical Systems and Signal Processing*, 2018, 106: 537–572.
[10] J C Fang, X B Xu, J J Xie. Active vibration control of rotor imbalance in active magnetic bearing systems. *Journal of Vibration and Control*, 2015, 21: 684–700.
[11] S Q Zheng, R Feng. Feedforward compensation control of rotor imbalance for high-speed magnetically suspended centrifugal compressors using a novel adaptive notch filter. *Journal of Sound and Vibration*, 2016, 366: 1–14.
[12] S Heindel, P C Müller, S Rinderknecht. Unbalance and resonance elimination with active bearings on general rotors. *Journal of Sound and Vibration*, 2018, 431: 422–440.
[13] S L Chen, S Y Lin, C S Toh, et al. Adaptive unbalance compensation for a three-pole active magnetic bearing system. *IEEE Transactions on Industrial Electronics*, 2020, 67(3): 2097–2106.
[14] X Shao, W M Wang, W B Li, et al. Active fast vibration control of rotating machinery via a novel electromagnetic actuator. *Structural Control Health Monitoring*, 2021, 28(5): e2707.
[15] J I Inayat-Hussain. Nonlinear dynamics of a statically misaligned flexible rotor in active magnetic bearings. *Communications in Nonlinear Science and Numerical Simulation*, 2010, 15: 764–777.
[16] S Bouaziz, N B Messaoud, M Mataar, et al. A theoretical model for analyzing the dynamic behavior of a misaligned rotor with active magnetic bearings. *Mechatronics*, 2011, 21(6): 899–907.
[17] P Kumar, R Tiwari. Finite element modelling, analysis and identification using novel trial misalignment approach in an unbalanced and misaligned flexible rotor system levitated by active magnetic bearings. *Mechanical Systems and Signal Processing*, 2021, 152: 107454.
[18] K J Jiang, C S Zhu. Multi-frequency periodic vibration suppressing in active magnetic bearing-rotor systems via response matching in frequency domain. *Mechanical Systems and Signal Processing*, 2011, 25(4): 1417–1429.
[19] J F Yao, J J Gao, W M Wang. Multi-frequency rotor vibration suppressing through self-optimizing control of electromagnetic force. *Journal of Vibration and Control*, 2017, 23(5): 701–715.
[20] M Zhen, Y S Tian, T Sun, et al. Nonlinear dynamics of two-span rotor-bearing system with flexible coupling misalignment. *Journal of Mechanical Engineering*, 2020, 56: 109–117. (in Chinese)
[21] S Arimoto, S Kawamura, F Miyazaki. Bettering operation of robots by learning. *Robotic System*, 1984, 1(2): 123–140.
[22] B T Costic, M S de Queiroz, D N Dawson. A new learning control approach to the active magnetic bearing benchmark system. *Proceedings of 2000 American Control Conference*, Chicago, IL, USA, June 28–30, 2000, 4: 2639–2643.
[23] H G Chiacchiarin, P S Mandolesi. Unbalance compensation for active magnetic bearings using ILC. *Proceedings of the 2001 IEEE International Conference on Control Applications*, Mexico City, Mexico, September 7, 2001: 58–63.
[24] C Bi, D Z Wu, Q Jiang, et al. Automatic learning control for unbalance compensation in active magnetic bearings. *IEEE Transactions on Magnetics*, 2005, 41(7): 2270–2280.
[25] H Gao, L X Xu, Y L Zhu. Unbalance vibratory displacement compensation for active magnetic bearings. *Chinese Journal of Mechanical Engineering*, 2013, 26(1): 95–103.
[26] Z Z Tang, Y J Yu, Z H Li, et al. Disturbance rejection via iterative learning control with a disturbance observer for active magnetic bearing systems. *Frontiers of Information Technology and Electronic Engineering*, 2019, 20: 131–140.
[27] Y B Zheng, N Mo, Y Zhou, et al. Unbalance compensation and automatic balance of active magnetic bearing rotor system by using iterative learning control. *IEEE Access*, 2019, 7: 122613–122625.
[28] Y B Zheng, N Mo, Y Zhou, et al. A model-free control method for synchronous vibration of active magnetic bearing rotor system. *IEEE Access*, 2019, 7: 79254–79267.
[29] X D Sun, Z J Jin, L Chen, et al. Disturbance rejection based on iterative learning control with extended state observer for a four-degree-of-freedom hybrid magnetic bearing system. *Mechanical Systems and Signal Processing*, 2021, 153: 107465.
[30] J F Yao, J B Dai, L Liu. Unbalanced vibration response reduction of rotor using active magnetic actuator based on PD control. *International Journal of Acoustic and Vibration*, 2019, 24(2): 327–333.
[31] S Arimoto, S Kawamura, F Miyazaki, et al. Learning control theory for dynamical systems. *24th IEEE Conference on Decision and Control*, Fort Lauderdale, USA, December 11–13, 1985: 1375–1380.

Yifan Bao born in 1996, is currently a master candidate at *Mechanical and Electrical Engineering, Beijing University of Chemical Technology, China*. His research interests include the design of rotor vibration active control algorithm and active magnetic bearings.

Jianfei Yao born in 1979, and obtained his PhD degree in Power Engineering and Engineering Thermophysics from *Beijing University of Chemical Technology, China*. He is currently a Professor at *Beijing Key Laboratory of High-end Mechanical Equipment Health Monitoring and Self-Recovery, Beijing University of Chemical Technology, China*. His research interests are in the field of rotor dynamics, vibration

control, fault diagnostics for rotating machinery, smart materials and structures, and mechanical metamaterials. He has authored more than 40 publications.

Fabrizio Scarpa obtained a PhD degree in Machine Design from *Politecnico of Torino, Italy*. He is currently a Professor at *Bristol Composites Institute (ACCIS), University of Bristol, UK*. His research activities span the field of mechanical metamaterials, auxetics (foams and honeycombs), Kirigami and shape memory alloy honeycombs, smart multifunctional cellular solids, viscoelasticity and structural-acoustic coupling. He has authored about 370 publications.

Yan Li born in 1980, and obtained the PhD degree in Control Science and Engineering from *Beijing University of Chemical Technology, China*. He is currently an associate Professor at *Beijing Key Laboratory of High-end Mechanical Equipment Health Monitoring and Self-Recovery, Beijing University of Chemical Technology, China*. His research interests are in the field of automatic control and vibration control.